Strojniški vestnik - Journal of Mechanical Engineering 64(2018)4, p. 209-215
DOI:10.5545/sv-jme.2017.5063
Original Scientific Paper
Received for review: 2017-11-08
Received revised form: 2018-02-26
Accepted for publication: 2018-03-19


# Analysis on Damage to Rolling Bearings at Small Turning Angles

Ivan Okorn* – Marko Nagode – Jernej Klemenc
University of Ljubljana, Faculty of Mechanical Engineering, Slovenia

*A test rig was developed for testing air springs. It uses the energy returned by the spring during unloading. The springs are loaded by means of a lever oscillating around its rotation point at a small angle. During operation, it was determined that rotation point bearings are critical elements of the test rig. This paper shows and analyses the damage that occurs on bearing ring raceways. Contact pressure and stress under individual rolling elements were calculated by using the finite element method (FEM). Mechanisms of the formation and propagation of damage were identified. Optical and electronic microscopy was used for confirming the mechanisms of damage formation. The microstructure of damaged material was analysed. It was found that depressions on bearing ring raceways form due to material fatigue and fretting. The required bearing replacement frequency was determined with respect to load.*

**Keywords: damage of rolling bearing, wear, partially-rotatory machines, false brinelling, fatigue, fretting**

**Highlights**

- *Damage to a rolling bearing in a partially-rotatory machine is shown.*
- *Failure mechanisms were found by using optical and electron microscopy.*
- *Load distribution on rolling elements was calculated by the FEM.*
- *Basic rating life till critical damage of a bearing was determined.*

## 0 INTRODUCTION

Bearings in joints of various mechanisms do not make a full 360-degree rotation. In such cases, tribological conditions between rolling elements and ring raceways are different than those in rotating bearings. A basic dynamic load rating is defined for standard bearings, and their basic rating life is determined by using ISO 281 [1]. Characteristic damage of rolling bearings were described and shown in papers [2] to [5]. Lubrication of bearing contact areas is not adequate in partially-rotatory machines, so critical damage occurs sooner than with rotating bearings [6]. Wear mechanisms are also different. Algorithms that are used for the evaluation of rotating bearings cannot be used for partially-rotatory machines. Producers of bearings do not recommend the use of rolling bearings for small turning angles. A minimum turn of the rotating ring should allow at least a full rotation of the rolling element.

The problem of small turning angles during the development of an air-spring test rig was encountered. The lever that presses the spring turns by a small angle (±2.5° to ±4°) in its rotation point, depending on settings. Both rolling and plain bearing versions of the rotating point were considered. The basic rating life is limited in both cases due to wear, which could be eliminated only by using hydrostatic bearings. This option was not selected because of its high cost and demanding construction. Finally, a rolling implementation of the rotation point was developed, despite the known lubrication problems with small turning angles. Friction losses are smaller in rolling implementation, and heat load of the rotation point is also smaller [7]. Energy efficiency of this test rig was analysed in paper [8]. Bearings were replaced when critical damage occurred, which caused increased noise and vibrations of the rotation point. Depressions formed under the rolling elements and, consequently, the bearing play increased

Damage and failures of rolling bearings are systematically described in ISO 15243 standard [9] and in handbooks of bearing manufacturers [10]. The primary failure modes are fatigue, wear, corrosion, electrical erosion, plastic deformation, and fracture and cracking. In static rolling bearings that operate under vibration, the so-called false brinelling damage can occur [11]. It is a form of corrosion-induced damage. Vibrations of the rolling element can push the lubricant out of the region of the touch between the rolling element and its raceway. This leads to a direct contact of two metal surfaces, to the destruction of the protective layer of natural oxides, and to fretting [12] and [13]. Damage to raceways occurs in the form of depressions. Shapes of depressions were shown in papers [14] and [15]. The lubricant can also be pushed out of two surfaces in contact when the rolling element turns at just a small angle. Such damage has been found in pitch and yaw bearings in wind turbines [16] and [17]. Similar depressions are caused by the plastic deformation that occurs at a sudden overload.

*Corr. Author's Address: University of Ljubljana, Faculty of Mechanical Engineering , Aškerčeva 6, 1000 Ljubljana, Slovenia, ivan.okorn@fs.uni-lj.si

Damage in bearings of the rotation point lever in the air-spring test rig also had the shapes of depressions. They appeared only on one half of the bearing ring: on a part that transferred forces. Depression depth depends on the load being transferred via individual rolling element. Load distribution on individual rolling elements was calculated by using the FEM. In the following chapters, the damage of the bearings will be shown, and the causes and propagation of the damage will be analysed.

## 1 FORCES ON THE BEARING

Fig. 1 schematically shows the loading of the spring. The eccentric mechanism with a rotation point 3 pushes the lever via a slider. The lever oscillates around its rotating point 5, thereby loading one spring and releasing the other one via inclined plates. Four springs are tested simultaneously. They are loaded with two eccentric mechanisms that are phase shifted by an angle of 90°. The spring that is being released returns the energy to the system, while the spring that is being compressed, uses the energy from the system. An electric motor drives the test rig; it provides the missing energy to compress the spring and energy to cover friction losses. The energy situation in the test rig was analysed in paper **[8]**.

The load of the bearings in the rotation point depends on the size of the spring, the geometric settings of the test rig, and the frequency of loading. A computer program that calculates cinematic parameters and the load of test rig components during a test of any spring was developed. The maximum turning angle of the lever $\varphi_{5\max}$ depends on the geometric settings of the test rig and ranges from ±2.5° to ±4°. Most of the tests are carried out at the angle of $\varphi_{5\max} = \pm 3.4°$ and at the loading frequency of 3.3 Hz.

Bearings in the rotation point are loaded radially by the resultant of forces $F_{5x}$ and $F_{5y}$. The forces change during the oscillation of the lever. They depend on working forces of the springs, weight and inertia of the lever. Reaction forces on the lever are shown in Fig. 1. Forces that act from the lever to the bearings are of equal size and in the opposite direction. The size of $F_{5x}$ component (but not its direction) changes due to the inclination of the spring. Rolling elements on one side of the bearing are always in contact with the raceways, in spite of increasing play during operation. Neglecting the lever weight, the bearing is symmetrically loaded with respect to the $x$-axis, and it is loaded only with the $F_{5x}$ component in its neutral (horizontal) position. When the locations of damage were checked, damage in the rings was symmetrical with respect to the $x$-axis.

## 2 STRESS AND CONTACT PRESSURE DISTRIBUTION

The lever is fixed to the axle in the rotation point 5, which is supported in a housing with two spherical roller bearings. The bearing with diameters $d = 80$ mm and $D = 140$ mm has a dynamic load rating $C = 236$ kN and static load rating $C_0 = 270$ kN. It has 21 rolling elements in two rows. During oscillation of

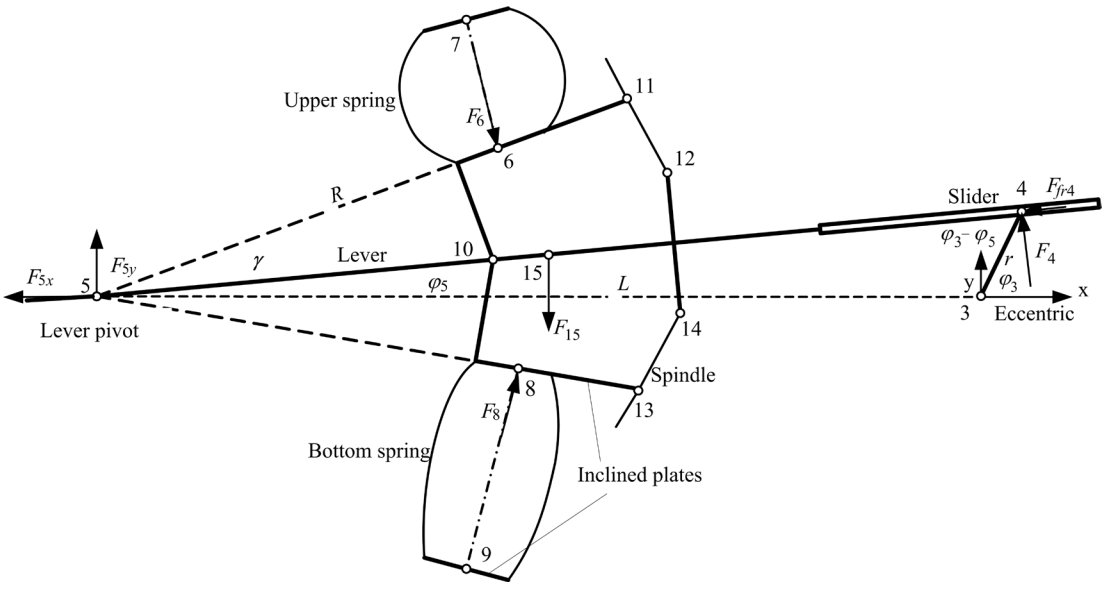


**Fig. 1.** *Loading of air springs*

the internal ring, the size and direction of a radial load changes, as well as the angular velocity of the ring and rolling elements. The actual radial force on the bearing varies from 8 kN to 18 kN. The positions of rolling elements are shown in Fig. 2.

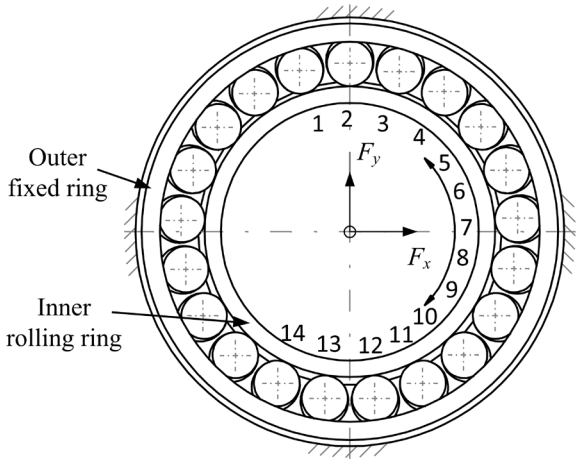


**Fig. 2.** *Positions of rolling elements and damage*

The distributions of contact pressure and von Mises stress have been calculated in two characteristic lever positions by using the FEM. In order to reduce the number of finite elements, only half of the width of the bearing was used in the calculation. The force was entered in the middle of the entire width of the bearing. The movement of rings was limited along the *z*-axis. Fig. 3 shows the stress in the bearing elements in a neutral position of the lever, while Fig. 4 shows the stress at the maximum turn of the lever.

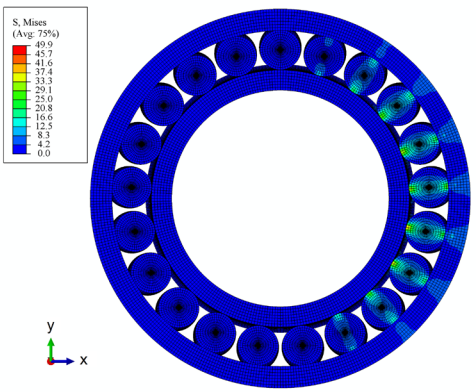


**Fig. 3.** *Von Mises stresses in MPa at $F_x$ =10 kN and $F_y$ = 0 kN*

Fig. 5 shows a distribution of Von Mises stresses along the depth of the inner ring. We selected the location with the highest stresses (position 5).

The pressure distribution on the surface of the internal ring raceway is shown in Figs. 6 and 7.

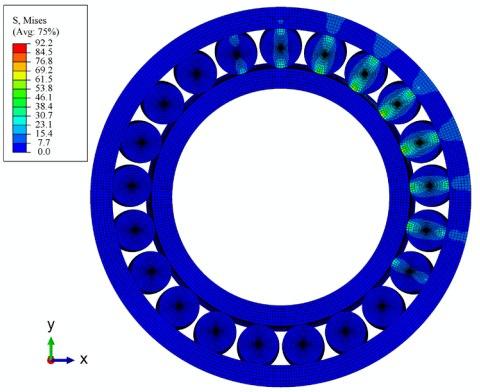


**Fig. 4.** *Von Mises stresses in MPa at $F_x$ =14 kN and $F_y$ = 10 kN*

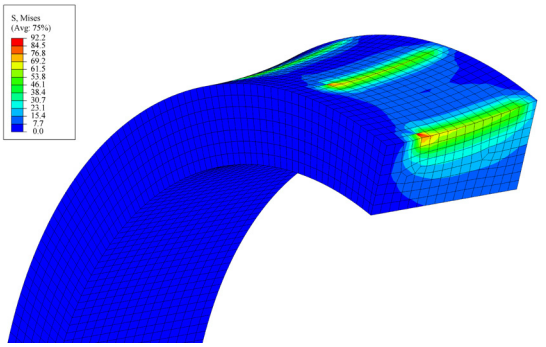


**Fig. 5.** *Distribution of stresses by depth at position 5 in MPa at $F_x$ =14 kN and $F_y$ = 10 kN*

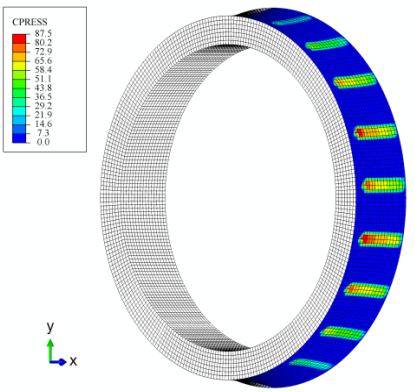


**Fig. 6.** *Contact pressure distribution in MPa at $F_x$ = 10 kN and $F_y$ = 0 kN*

The pressure distribution on the other raceway is symmetrical with respect to a plane passing through the middle of the bearing.

The purpose of the FEM analysis was to determine the load distribution on the bearing ring and to determine the maximum pressure and stress. By comparing the actual stress and the yield strength of the 100Cr6 bearing steel (ISO 683-17 notation), the

probability of plastic deformation at the macro level was determined. The yield strength of the 100Cr6 steel is about 1300 MPa. The actual highest stress is thus about 14 times smaller than the yield stress of the bearing steel. On the basis of the FEM analysis it was concluded that the plastic deformation of raceways at the macro level was not possible.

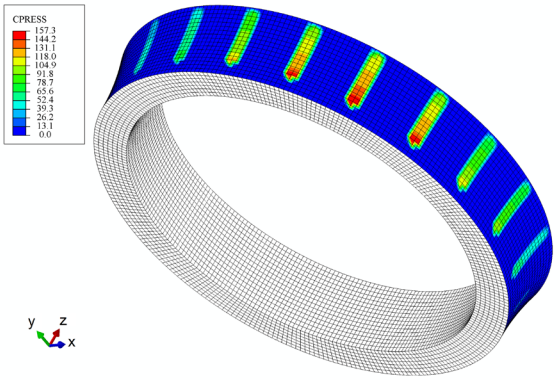


**Fig. 7.** *Contact pressure distribution in MPa at $F_X$ = 14 kN and $F_y$ = 10 kN*

## 3 TEST RESULTS AND DISCUSSION

The damage that occurred after three months of the test rig operation at the testing frequency of 3.3 Hz was analysed. Damage occurred under thirteen rolling elements, both on the outer and inner bearing rings. Depressions are deeper on the internal ring. The change of the diameter of the rolling elements is negligible. Only a trace of a contact with a rolling element can be seen under the first and last rolling element, without a significant material removal. Depressions of various depths can be seen under all other rolling elements.

Depression depth increases from the second to seventh rolling element and then decreases. Depressions on the internal ring are shown in Fig. 8. Fig. 8a shows how damage depth increases under individual rolling elements. The location and extent of the damage is consistent with the distribution of load on the individual rolling elements. Deeper depressions formed under the elements that are loaded continuously.

In order to determine the source of damage, the damage at the surface of the internal raceway at the first, third, fifth, and seventh rolling element was analysed. Surface damage was examined using optical and electron microscopes. The bearing ring was then cut across its width, and the condition of the material (cracks, microstructure) under the surface of damage was reviewed. The microhardness $HV_{0.1}$ under the damage was measured up to the depth of 1 mm.

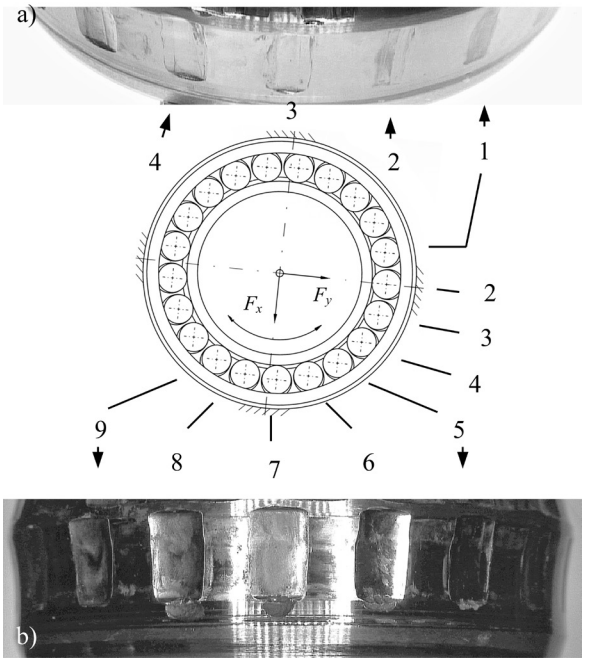


**Fig. 8.** *Defect at the surface of the raceway; a) damage depth under individual rolling elements 1 to 4, b) damage depth under rolling elements 5 to 9*

Only a trace of the rolling element can be seen on the internal raceway at the first rolling element, while the first traces of material removal can be seen at the third one. The damage at elements 3 to 7 is similar, with the extent of damage becoming larger. Damage 1 is shown in Fig. 9. When the surface was examined with an optical microscope, cracks were detected in the direction of the roll. Electron microscopy confirmed the fatigue cracks.

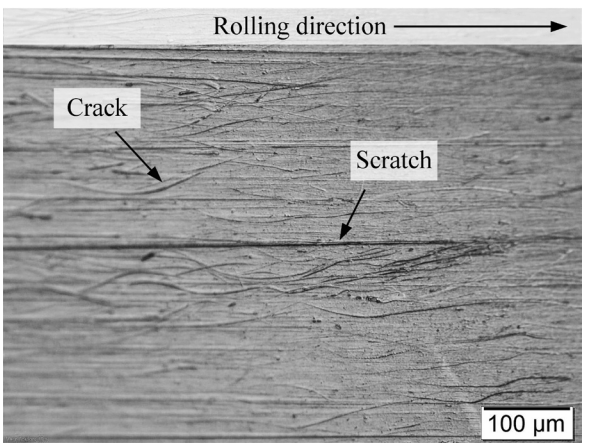


**Fig. 9.** *Damage 1; cracks on the surface*

In the case of damage 3, the progression of the surface fatigue is visible, with a typical surface full of small pits (Fig. 10). Progression of cracks can be seen in some parts of damage 3 (Fig. 11). There are no oxidation products that would indicate fretting.

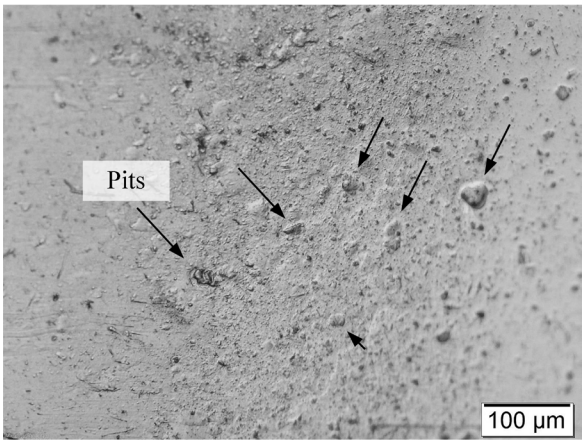


**Fig. 10.** *Damage 3; pitting of the surface*

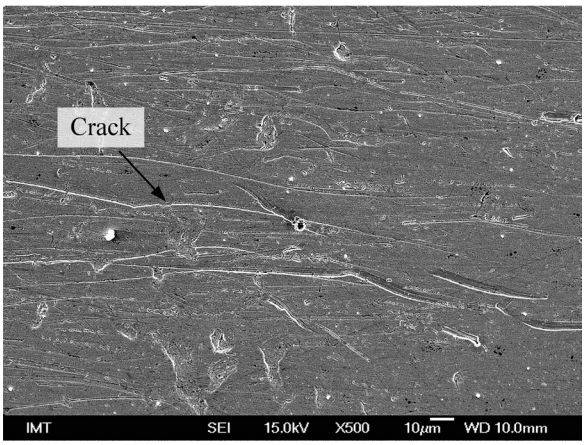


**Fig. 11.** *Damage 3; progression of cracks*

Damage 5 is deeper and wider than damage 3. The surface of the damage is shown in Fig. 8b. Pronounced removal of material with pitting can be seen in Fig. 12. Tribocorrosion and fretting wear occur on locations of pitting due to the uncovering of the metal surface. The wear mechanism is similar in damage 7, with the extent of damage being larger. Tribocorrosion is confirmed by the presence of red-brown surface areas. The presence of oxides was confirmed by electronic microscopy (Fig. 13). Oxides are harder than the surface material, so they act as abrasive particles between the roller and the raceway. The intensity of wear, therefore, increases further.

Each of the treated damaged samples was cut transversely. Figures showing the crack propagation under the surface confirm the mechanism of fatigue. Widening of one of the cracks can be seen in Fig. 14.

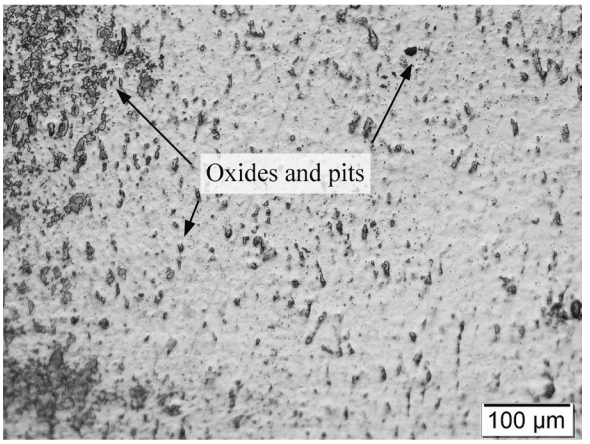


**Fig. 12.** *Surface of damage 5*

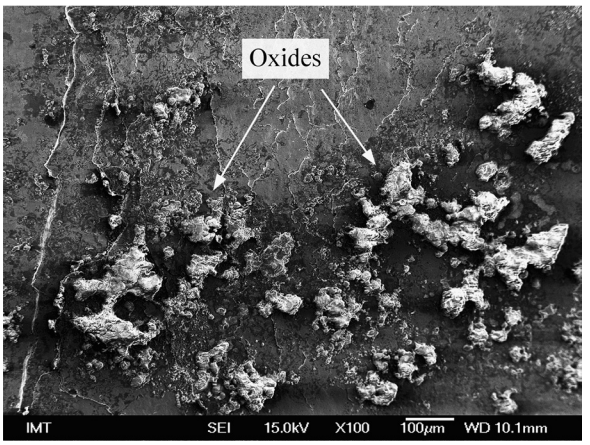


**Fig. 13.** *Oxides on the surface of the damage*

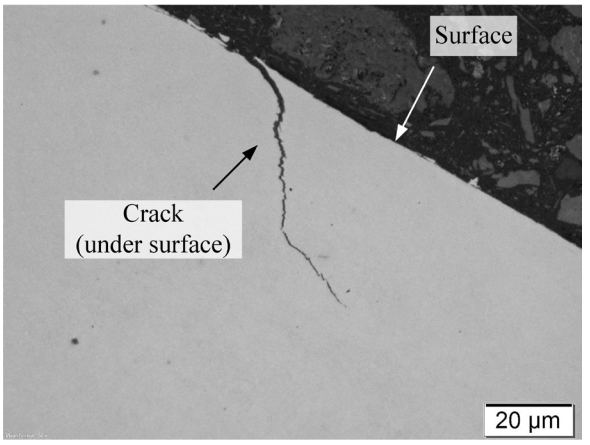


**Fig. 14.** *Propagation of cracks under the surface*

Microstructures in the core and under the damaged area in the cross section of metallographically prepared samples were compared. It can be seen from Fig. 15

that the microstructure is the same. This proves that the load of the contact area did not exceed the yield point, and there was no macro plastic deformation of the material.

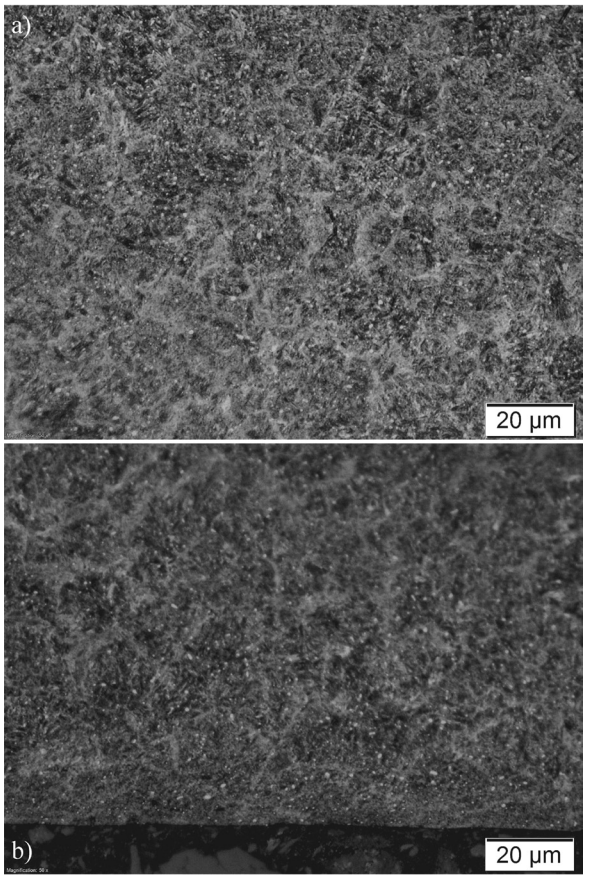


**Fig. 15.** *a) Core microstructure, b) microstructure under the surface of the damage*

Distribution of microhardness of the material under the damage is shown in Fig. 16 for all four instances of damage that are the subject of this discussion. It can be seen from the profile that the surface does not become harder, which would be typical for the overload and makro plastic deformation of the surface of the bearing steel. A drop of hardness in the surface layer (50 µm micrometers to 100 µm thick) can be seen in all four instances of damage. A larger drop of hardness and the thickness of the layer with the reduced hardness are present at the early instances of damage (1 and 3). This indicates that a contact temperature increased (> 200 °C), which could lead to tempering of the material surface. The higher surface hardness at instances of damage 5 and 7 may be caused by the secondary hardening of the surface after the peeling.

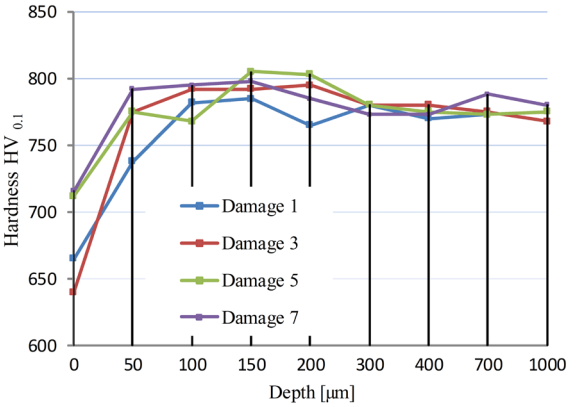


**Fig. 16.** *Microhardness under instances of damage*

## 4 CONCLUSIONS

This paper analyses damage to a spherical bearing in a test rig for air springs. The test rig was constructed in the laboratory of an air spring manufacturer, and it operates there. The ring of the rolling bearing oscillates by a small angle in the rotation point of the lever. After two months of uninterrupted operation, damage in the form of depressions appeared on bearing ring raceways. Vibrations of the test rig increased due to this damage, and bearings had to be replaced.

The defects were examined using optical and electron microscopes. The main cause of wear was determined to be material fatigue. Cracks and small pits are clearly visible on surfaces of depressions. We have proven the occurrence of cracks and crack propagation into the depth of the material. The surface under the most loaded rolling elements is red-brown, which indicates fretting. The presence of oxides was confirmed using electronic microscopy. The damage propagation was even more intense under the critically loaded rolling elements just because of the fretting wear.

FEM calculation of stress and roller pressure shows that the stress and pressure are far below the yield strength of the 100Cr6 bearing steel. Examination of the microstructure under the surface of the damage revealed that it is identical to the microstructure in the core. Microhardness does not change significantly in depth, which indicates that the surface does not harden. Thus, we have proven that depressions were not caused by the plastic deformation of the material. Depressions were formed due to removal of material, which was caused by several wear mechanisms. When using the term "plastic deformation", we have in mind the deformation on a macro level. During operation, plastic deformation of the surface irregularities occurs

on a micro level: pits and scratches on the surface are getting smoother. We also have not detected that the material would be pushed onto the edge of depressions.

A practical use of a spherical bearing proves that rolling bearings are not suitable for small turning angles. Depressions under the rolling elements form at very low loads. If rolling bearings are used in the rotation point, they must be replaced after two to three months of operation, depending on the settings of the test rig. Due to the favourable direction of the bearing load, even relatively deep damage still allows functional operation of the test rig. We have also developed a rotation point with a plain bearing. A sliding solution is more favourable from the maintenance perspective, since the sliding bushing must be changed only twice a year.

## 5 ACKNOWLEDGMENTS

We would like to thank to the Institute of Metals and Technology (Ljubljana, Slovenia) for producing photographs of damage and microstructure, and for microhardness measurements. The authors acknowledge the financial support from the Slovenian Research Agency (research core funding No. P2-0182).

## 6 REFERENCES

[1] ISO 281:2007 (2007). *Rolling Bearings - Dynamic Load Ratings and Rating Life*. International Organisation for Standardization, Geneva.

[2] El-Thalji, I., Jantunen, E. (2014). A descriptive model of wear evolution in rolling bearings. *Engineering Failure Analysis*, vol. 45, p. 204-224, **DOI:10.1016/j.engfailanal.2014.06.004**.

[3] Carroll, R.I., Beynon, J.H. (2007). Rolling contact fatigue of white etching layer: Part 1: Crack morphology. *Wear*, vol. 262, no. 9-10, p. 1253-1266, **DOI:10.1016/j.wear.2007.01.003**.

[4] Gagg, C.R., Lewis, P.R. (2007). Wear as a product failure mechanism – Overview and case studies. *Engineering Failure Analysis*, vol. 14, no. 8, p. 1618-1640, **DOI:10.1016/j.engfailanal.2006.11.064**.

[5] Gurumoorthy, K., Ghosh, A. (2013). Failure investigation of a taper roller bearing: A case study. *Case Studies in Engineering Failure Analysis*, vol. 1, no. 2, p. 110-114, **DOI:10.1016/j.csefa.2013.05.002**.

[6] Upadhyay, R.K., Kumaraswamidhas, L.A., Sikandar Azam, Md. (2013). Rolling element bearing failure analysis: A case study. *Case Studies in Engineering Failure Analysis*, vol. 1, no. 1, p. 15-17, **DOI:10.1016/j.csefa.2012.11.003**.

[7] Blanuša, V., Zeljković, M., Milisavlevich, B.M., Savić, B. (2017). Mathematical modelling of thermal behaviour of cylindrical roller bearing for towed railway vehicles. *Tehnički vjesnik - Technical Gazette*, vol. 24, suppl. 1, p. 211-217, **DOI:10.17559/TV-20150809184241**.

[8] Okorn, I., Nagode, M. (2015). Analysis of energy efficiency of a test rig for air springs. *Strojniški vestnik – Journal of Mechanical Engineering*, vol. 6, no. 1, p. 53-62, **DOI:10.5545/sv-jme.2014.2143**.

[9] ISO 15243:2017 (2017). *Rolling bearings – Damage and Failures – Terms, Characteristics and Causes*. International Organisation for Standardization, Geneva.

[10] SKF Group. (2012). *Bearing investigation. Railway Technical Handbook*. vol. 1, Chapter 6, SKF, Göteborg

[11] Phaner-Goutorbe, M., Barthou, C., Porte, L., Vannes, B. (1997). Scanning tunneling microscopy study of wear induced by false brinelling on rolling bearings. *Applied Surface Science*, vol. 108, no. 1, p. 45-51, **DOI:10.1016/S0169-4332(96)00571-5**.

[12] Barthou, C., Vannes, B., Girodin, D., Pierantoni, M., Sauger, E. (1998). Methodology of characterisation of the raceway / lubricant / ball contacts submitted to vibrations and degraded by false brinelling. *Tribology Series*, vol. 34, p. 389-398, **DOI:10.1016/S0167-8922(98)80095-3**.

[13] Varenberg, M., Halperin, G., Etsion, I. (2002). Different aspects of the role of wear debris in fretting wear. *Wear*, vol. 232, no. 11-12, p. 902-910, **DOI:10.1016/S0043-1648(02)00044-3**.

[14] Warmuth, A.R., Pearson, S.R., Shipway, P.H., Sun, W. (2013). The effect of contact geometry on fretting wear rates and mechanisms for high strengthsteel, *Wear*, vol. 301, no. 1-2, p. 491-500, **DOI:10.1016/j.wear.2013.01.018**.

[15] Massi, F., Rocchi, J., Culla, A., Berthier, Y. (2010). Coupling system dynamics and contact behaviour: Modelling bearings subjected to environmental induced vibrations and 'false brinelling' degradation. *Mechanical Systems and Signal Processing*, vol. 24, no. 4, p. 1068-1080, **DOI:10.1016/j.ymssp.2009.09.004**.

[16] Kotzalas, N.M, Doll, G.L. (2010). Tribological advancements for reliable wind turbine performance. *Philosophical Transactions of the Royal Society A*, vol. 368, no. 1929, p. 4829-4850, **DOI:10.1098/rsta.2010.0194**.

[17] Greco, A., Sheng, S., Keller, J., Erdemir, A. (2013). Material wear and fatigue in wind turbine Systems. *Wear*, vol. 302, no. 1-2, p. 1583-1591, **DOI:10.1016/j.wear.2013.01.060**.